
Gaia DR2 and EDR3 data and evolutionary status of post-AGB stars with high radial velocities

Wako AOKI^{1 2}, Tadafumi MATSUNO³ and Mudumba PARTHASARATHY^{1 4 5}

¹National Astronomical Observatory, 2-21-1 Osawa, Mitaka, Tokyo 181-8588, Japan

²Department of Astronomical Science, School of Physical Sciences, The Graduate University of Advanced Studies (SOKENDAI), 2-21-1 Osawa, Mitaka, Tokyo 181-8588, Japan

³Kapteyn Astronomical Institute, University of Groningen
Landleven 12, 9747 AD Groningen, The Netherlands

⁴Indian Institute of Astrophysics, II Block, Koramangala, Bangalore 560 034, INDIA

⁵Department of Physics and Astronomy, Vanderbilt University, Nashville, TN 37235, USA

*E-mail: aoki.wako@nao.ac.jp, matsuno@astro.rug.nl, m-partha@hotmail.com

Received (reception date); Accepted (acceptation date)

Abstract

Using the *Gaia* DR2 and EDR3 data and list of post-AGB candidates, we investigate the parallax, proper motion and binarity for twenty post-AGB stars and candidates having high radial velocities. From their *Gaia* distances their luminosities and kinematics are derived. The evolutionary status of these stars is discussed from their location on the post-AGB evolutionary tracks. Nine stars are confirmed to be post-AGB stars that have their initial main-sequence mass around one or two solar masses. From their kinematics information, two objects among them are identified to clearly belong to the halo population, suggesting that low-mass. We discuss on the origin and evolutionary status of other objects in the sample of this work with high radial velocities.

Key words: stars:evolution — stars:AGB and post-AGB — stars:high-velocity — stars:distances

1 Introduction

Post-AGB stars are transition objects evolving from the tip of the AGB horizontally towards the left in the H-R diagram into early stages of young planetary nebulae (PNe). The post-AGB evolutionary stage is short-lived, depending on the core-mass (Schoenberner 1983; Iben & Renzini 1983). During the transition from the tip of the AGB to early stages of young PNe phase they appear as M-,K-, G-, F-, A-, and OB-type post-AGB supergiants for a short period (Parthasarathy & Pottasch 1986; Parthasarathy & Pottasch 1989; Pottasch & Parthasarathy 1988; Parthasarathy 1993a; Parthasarathy 1993b). They mimic the spectra of supergiants because of their extended thin atmospheres around the white-dwarf like C-O core (after severe mass-loss and the termination of the AGB phase of evolution). Before the advent of IRAS satellite, very few post-AGB supergiant candidates were known. Analysis of IRAS data has revealed many cool to hot post-AGB supergiants (Preite-Martinez 1988; Kwok et al. 1989). The list of post-AGB stars detected from the analysis of IRAS data by several investigators can be found in the paper of Vickers et al. (2015) and references therein. Progresses in understanding of post-AGB stars are found in review papers (e.g., van Winckel 2003; Kamath & Van Winckel 2022).

Multi-wavelength studies of significant sample of post-AGB candidates were carried out by several investigators during the past 35 years which enabled us to understand their chemical composition, circumstellar shells, s-process nucleosynthesis and late stages of evolution of low-mass stars (e.g., De Smedt et al. 2012; De Smedt et al. 2016; Kamath et al. 2022; Parthasarathy 2022, and references therein). However, for a better understanding of these stars, their distances, radial velocities and accurate proper-motion measurements are required. With the advent of *Gaia* (DR2 and EDR3; Gaia Collaboration et al. (2018); Lindegren et al. (2018)), accurate parallaxes(distances), radial velocities and proper-motions measurements of a large sample post-AGB stars became available.

In an earlier paper (Parthasarathy et al. 2020), we studied the Gaia DR2 data and evolutionary status of eight high velocity hot post-AGB stars. Finding high-velocity objects among post-AGB stars is useful to constrain the final stage of stellar evolution of low-metallicity, low-mass stars in the halo population. Such stars are very rare and are old low-mass stars in advanced stages of evolution. Some of them may belong to the Galactic halo. In this paper we present an analysis of *Gaia* DR2 and EDR3 data of stars listed as post-AGB stars or candidates in literature.

2 Data and analysis

We investigate the list of stars given in the paper of Vickers et al. (2015) as likely or possibly post-AGB stars, and searched the *Gaia* DR2 and EDR3 for post-AGB stars with radial velocities and with accurate parallaxes. The sample of Vickers et al. (2015) contains the list of almost all the known post-AGB stars. Here we define post-AGB stars as those which are in the transition region between the tip of the AGB and very early stages of planetary nebulae (PNe). These objects are often termed as proto-planetary nebulae.

We select 20 objects that have absolute values of radial velocities larger than 45 km s^{-1} ($|RV| > 45 \text{ km s}^{-1}$). The galactic longitudes and latitudes, parallaxes, radial velocities, G (*Gaia* G band magnitude), V , $(B - V)$ and Spectral types are given in tables 1 and 2. Spectral types, V , B magnitudes are taken from SIMBAD. Among the twenty stars twelve are high galactic latitude stars, eleven stars have high negative radial velocities and nine have high positive radial velocities.

The parallaxes taken from *Gaia* DR2 and EDR3 are given in table 2. The distance derived from the parallaxes are also listed in the table. Four stars have a large relative parallax uncertainty ($>20\%$) in *Gaia* EDR3. For these stars, only the lower limit of the distance is presented. The table also gives the distances estimated by Bailer-Jones et al. (2021) using a prior constructed from a three-dimensional model of the Galaxy. Excluding the above four objects, the two estimates of the distance for each object agree within 5%. We adopt the distances simply obtained from the parallaxes in the present work.

The normalized unit weight error (RUWE) values are also given in the table. The RUEW values also indicate reliability of the parallaxes. Whereas RUWE values are sensitive to the photocentric motions of unresolved companions (Lindgren et al. 2021; Stassun & Torres 2021), they could be affected by other factors including nebulosity of proto planetary nebulae. The RUWE values of nine stars, including the above four objects with large uncertainties of parallaxes, are larger than 1.4. Among them, four objects are likely to be post-AGB stars according to previous studies on stellar properties including infrared excess, and metal depletion. See below more details on these stars. The remaining five stars have large uncertainties in parallaxes and/or very large RUWE values, and, hence, are not regarded as candidates of post-AGB stars in this paper.

The other eleven stars in our sample have RUWE values smaller than 1.4. Among them, BD+33 2642 is suggested to belong a binary system (Van Winckel et al. 2014). For the remaining ten objects, there is no signature of binarity from the *Gaia* astrometry.

The kinematic information that is calculated based on the *Gaia* EDR3 astrometry is presented in table 3, excluding the four objects with large uncertainties of parallaxes.

$E(B - V)$ values are obtained from dust maps in literature or by comparing expected intrinsic colors with observed ones (table 1). We use three-dimensional dust extinction map from Chen et al. (2019) and Green et al. (2018) and two-dimensional dust extinction map from Schlegel et al. (1998). For a star to have an $E(B - V)$ estimate from three-dimensional maps, it needs to have a precise parallax measurement (relative uncertainty smaller than 20%) and be in the sky coverage of the maps. Since Chen et al. (2019) focus on low Galactic latitude field ($|b| < 10^\circ$), we prioritize values from Chen et al. (2019) over Green et al. (2018) for objects with $|b| < 10^\circ$. We note that Green et al. (2018) only covers the sky with declination larger than -30° and hence we could not derive $E(B - V)$ from three-dimensional maps for HD 16745 and HD 178443 despite precise parallax measurements available for these objects. The extinction coefficients from Green et al. (2018) and Chen et al. (2019) are converted to $E(B - V)$ using values provided in Green et al. (2018), Schlafly, & Finkbeiner (2011), and Casagrande et al. (2019). In addition to the interstellar extinctions considered in these dust maps, some objects could be affected by circumstellar dust extinction given the evolutionary status of the objects. Thirteen objects are indeed IRAS sources and their $(B - V)$ colours are likely affected by circumstellar reddening. For instance, the $E(B - V)$ of HD 56126 (IRAS 07134+1005) estimated from the spectral type is 0.56, whereas the $E(B - V)$ from the dust map is quite small (0.08 or less). For these stars we used the observed $(B - V)$ values from SIMBAD and intrinsic $(B - V)_0$ values estimated from their spectral types using Table 15.7 of Allen’s Astrophysical Quantities (Cox 2000) with interpolation to derive $E(B - V)$ values. The $E(B - V)$ values derived in this way are prioritized over the values from dust maps.

On the other hand, the $E(B - V)$ values of IRAS 07140-2321, IRAS 07227-1320, and IRAS 14325-2321 estimated from the spectral types are significantly smaller than those from the dust map. This suggests that the estimate of the reddening from the dust map or spectral types could be uncertain for these objects. For these three stars, we adopt $E(B - V)$ from the dust map.

The typical errors of $E(B - V)$ from the dust map is 0.02–0.03 for high Galactic latitude objects. We adopt 0.05 as the uncertainty of reddening of these objects to determine the luminosity. This is consistent with the error of $E(B - V)$ given in Vickers et al. (2015) for our sample (0.043 on average). For objects with large reddening, in particular objects that could be affected by circumstellar reddening, we assume the error of $E(B - V)$ to be 0.2, including the uncertainty of the subclass of spectral types that results in difference of $E(B - V)$. The

$E(B - V)$ and the error adopted are given in table 1. Taking the errors into account, the $E(B - V)$ values estimated in this study agree well with those obtained for HD 56126 (0.43) and IRAS 14325–6428 (1.07) by Kamath et al. (2022). Although our values are slightly larger than those for IRAS 05208–2035 (0.01) and HD 46703 (0.23) by Oomen et al. (2018), and for IRAS 08187–1905 (0.07) and HD 161796 (0.13) by Kamath et al. (2022), the discrepancy is smaller than 0.1. if the error ranges are taken into account.

The absolute V magnitudes are calculated from the apparent magnitudes and distances given in tables 1 and 2, respectively. The luminosity is calculated from the absolute magnitude and the bolometric corrections taken from Cox (2000). The values of bolometric corrections in Flower (1996) are 0.1–0.25 mag larger than those of Cox (2000), resulting in differences in $\log(L/L_{\odot})$ of less than 0.1 dex. The changes of $E(B - V)$ of 0.05 and 0.2 result in the difference of $\log(L/L_{\odot})$ of 0.08 and 0.25, respectively. The T_{eff} values and spectral types of most stars are available from the literature. These values are given in Table 2.

Kinematics are calculated using the *Gaia* EDR3 parallaxes and proper motion measurements. We adopt 8.21 kpc as the distance between the Sun and the Galactic center (McMillan 2017) and 0.021 kpc as the vertical offset of the Sun (Bennett & Bovy 2019). Solar motion is adopted from Schönrich et al. (2010) for radial and vertical velocities (11.1 km s⁻¹ and 7.25 km s⁻¹, respectively) and is calculated as 245.34 km s⁻¹ using proper motion measurements by Reid and Brunthaler (2004). The orbital energy is calculated assuming the Milky Way potential from McMillan (2017). These results are given in table 3. Kinematics of the post-AGB star candidates in Galactocentric frame are presented in figure1.

We note that the sample selection of high velocity post-AGB stars would not be affected if they belong to low mass binaries because the radial velocity variations expected for low mass binaries are not as large as the radial velocities of the stars studied in this paper (tables 1 and 2).

3 Notes on the twenty high velocity post-AGB candidates

Figure 2 shows the luminosity of the objects as a function of effective temperature with the post-AGB evolution tracks (Miller Bertolami 2016). The four objects with large uncertainties in the parallaxes (see § 2) are excluded. This figure indicates that typical luminosity range of low-mass post-AGB stars is $3 < \log(L/L_{\odot}) < 4$.

We find that nine objects have luminosity of this range, among which five have reliable *Gaia* parallaxes (the RUWE values are smaller than 1.4). BD–12 4970 that has very high

luminosity ($\log(L/L_{\odot}) = 5.5$) is also regarded as a post AGB star. Among the remaining ten stars with higher or lower luminosity than the above post-AGB star range, five with small RUWE have lower luminosity $\log(L/L_{\odot}) < 3$ and the other five have large RUWE values.

Here we report some detailed information for individual objects separately with the above grouping. It should be noted that the luminosities of binary stars are still uncertain due to the uncertainty of parallaxes. Although most of them are found in the groups with large RUWE values in this section, some known binary stars are also included in the groups with small RUWE values. Information on the binarity is given in the following notes for individual objects when available.

3.1 Post-AGB stars with small RUWE values

- HD 56126 (IRAS 07134+1005)

It is a high Galactic latitude, and high velocity, metal-poor, F-type post-AGB star with 21-micron emission feature. It is overabundant in carbon and s-process elements (Parthasarathy et al. 1992). De Smedt et al. (2016) report detailed abundances including $[\text{Fe}/\text{H}] = -0.91$ and large excesses of s-process elements (e.g., $[\text{Ba}/\text{Fe}] = 1.82$). More recently, Kamath et al. (2022) list this object as a single post-AGB star with s-process enrichment.

- IRAS 07140-2321 (V421 CMa)

Gielen et al. (2011) derived $T_{\text{eff}} = 7000$ K, $\log g = 1.5$, and $[\text{Fe}/\text{H}] = -0.8$.

- HD 116745 (CD-46°8644, Fehrenbach's star, ROA 24,)

It is a high galactic latitude and high velocity metal-poor halo post-AGB star (Gonzalez & Wallerstein 1992). They found it to be overabundant in carbon and s-process elements. They derived $T_{\text{eff}} = 6950$ K, $\log g = 1.15$ and $[\text{Fe}/\text{H}] = -1.77$. It is a member of the globular cluster Omega Cen.

- IRAS 17436+5003 (HD 161796)

It is a high galactic latitude and high velocity F-type post-AGB supergiant (Parthasarathy & Pottasch 1986). Luck et al. (1990) derived $T_{\text{eff}} = 6500$ K, $\log g = 0.70$, and $[\text{Fe}/\text{H}] = -0.32$. This object is listed as a single post-AGB star without s-process enrichment by Kamath et al. (2022).

- BD-12°4970 (LS IV -12 13)

It is a high velocity hot (B0.5Ia) post-AGB candidate. It is not an IRAS source. High resolution spectroscopic study of this star is important.

- BD+33 2642

It is a high Galactic latitude and high velocity, metal-poor hot post-AGB star. This object is also classified into a proto planetary nebula. However, its nebula is not bright, and it is not an IRAS source. Napiwotzki et al. (1994) studied this star and derived $T_{\text{eff}} = 20,000$ K, $\log g = 2.9$, and $[\text{Fe}/\text{H}] = -2.0$. Its chemical composition indicates depletion of refractory elements. The $[\text{O}/\text{H}] = -0.8$ indicates it is intrinsically metal-poor. This star belongs to a binary system with a low-mass faint companion. High resolution spectrum shows no spectral features of the secondary. The orbital period determined by Van Winckel et al. (2014) is 1105 days. The binarity of this object would not affect the RUWE value, which is smaller than 1.4 (1.295).

3.2 Post-AGB stars and candidates with large RUWE values

- HD 46703 (IRAS 06338+5333)

This star is a high Galactic latitude, and high velocity, metal-poor F-type pop II post-AGB star (Luck & Bond 1984). Luck & Bond (1984) derived $T_{\text{eff}} = 6000$ K, $\log g = 0.4$, $[\text{Fe}/\text{H}] = -1.57$. Parthasarathy & Pottasch (1986) were the first to find that it is a weak IRAS source with far-IR colours and flux distribution similar to that of high Galactic latitude post-AGB star HD 161796 (Parthasarathy & Pottasch 1986). Hrivnak et al. (2008) also report $[\text{M}/\text{H}] = -0.6$ for this object, discussing depletion and binarity. This belongs to a binary system. Oomen et al. (2018) report the orbital period of 597 days for this object. The RUWE value of this star is 1.622, which is clearly higher than 1.4 as expected from the binarity.

- IRAS 08187-1905 (HD 70379, V552 Pup)

It is a high galactic latitude and high velocity F6 post-AGB supergiant (Reddy & Parthasarathy 1996). Reddy & Parthasarathy (1996) derived chemical composition of this star from an analysis of high resolution spectra. They derived $T_{\text{eff}} = 6500$ K, $\log g = 1.0$, $[\text{Fe}/\text{H}] = -0.5$. This star is listed as a single post-AGB star without s-process enrichment by Kamath et al. (2022). The RUWE value of this object is 1.695, which is even higher than that of HD 46703. Although this would not indicate that this object belongs to a binary system, further investigation on the binarity will be useful.

- IRAS 14325-6428

It is a high velocity F5I star with IRAS colours and flux distribution similar to post-AGB stars and PNe. De Smedt et al. (2016) report $[\text{Fe}/\text{H}] = -0.56$ with excesses of s-process elements. This star is also regarded as a single post-AGB star without s-process enrichment by Kamath

et al. (2022). The RUWE value of this object is quite large (2.181). Whereas further study to investigate the binarity would be useful, this star can be treated as a post-AGB star with excesses of s-process elements according to literature.

- HD 137569 (IRASF 15240+1452)

It is a high Galactic latitude and high velocity post-AGB star. No Fe lines are detected in its spectrum by Martin (2004) and Martin (2006), who classified it as a metal-poor, hot post-Horizontal Branch (post-HB) star.

3.3 Objects with low luminosity with small RUWE

- IRAS 07227-1320

This star is listed as a possible post-AGB star by Vickers et al. (2015). Its spectral type is M1I. No chemical composition study is available. The luminosity of this object ($\log(L_*/L_\odot) = 2.58$) is lower than post-AGB stars in our sample.

- BD+32 2754

This star is also listed as a possible post-AGB star by Vickers et al. (2015). It is a high Galactic latitude and high velocity F-type star. There is no chemical composition analysis of this star. It may belong to Galactic halo. The luminosity of this object ($\log(L_*/L_\odot) = 1.10$) is clearly lower than post-AGB stars.

- HD 178443 (LSE 182)

It is not an IRAS source. It is a high Galactic latitude and high velocity (343.5 km s^{-1}) star. McWilliam et al. (1995) derived $T_{\text{eff}} = 5180 \text{ K}$, $\log g = 1.65$, $[\text{Fe}/\text{H}] = -2.07$. They classify it as a red-HB star. It is a Galactic halo star (see next section). The luminosity of this object ($\log(L_*/L_\odot) = 1.99$) is lower than post-AGB stars in our sample.

- PHL 1580

It is a high Galactic latitude and high velocity hot post-AGB star. McCausland et al. (1992) derived $T_{\text{eff}} = 24,000 \text{ K}$, $\log g = 3.6$, $[\text{Fe}/\text{H}] = -0.6$. They find it to be carbon deficient. This star may have left the AGB before the third dredge up. The luminosity of this object ($\log(L_*/L_\odot) = 1.12$) is clearly lower than post-AGB stars.

- LS III +52 5

It is a high velocity (-232.8 km s^{-1}) and high proper motion star. In the LS catalogue its spectral type is given as OB- (Hardorp et al. 1964). It is not an IRAS source. Detailed spectroscopic study of this star is important. The luminosity of this object ($\log(L_*/L_\odot) = 1.22$) is clearly lower than post-AGB stars.

3.4 Others with uncertain luminosity and large RUWE

- IRAS 02143+5852

It is a high radial velocity F7Iae star. The $H\alpha$ line is in emission. T_{eff} is estimated from its spectral type to be 6000K. Fujii et al. (2002) made *BVRIJHK* photometry. Omont et al. (1993) classified it as a carbon-rich post-AGB star. The error in parallax is large (tables 1 and 2).

- IRAS 05089+0459

It is a high galactic latitude and high velocity M3I post-AGB candidate. Iyengar & Parthasarathy (1997) made near-IR photometric observations ($R = 12.68$, $I = 11.62$). There is no chemical composition analysis of this star. The error in *Gaia* EDR3 parallax is high (tables 2).

- IRAS 05208-2035 (BD−20°1073, AY Lep)

It is a high Galactic latitude and high velocity post-AGB candidate. Gielen et al. (2011) derived $T_{\text{eff}} = 4000$ K, $\log g = 0.5$, and $[\text{Fe}/\text{H}] = 0.0$. The observed $B - V$ colour indicates that it may be a G-type star. The spectral type is not available in SIMBAD. On the other hand, $[\text{Fe}/\text{H}] = -0.7$ and small overabundance of s-process elements are derived by Rao et al. (2012). Oomen et al. (2018) derive the orbital period of this binary system to be 23 days. Although the luminosity of this star is still uncertain, it is likely to be a binary post-AGB star.

- IRAS 15210-6554

From *Gaia* DR2 data we find it to be a high velocity star. Its spectral type is K2I and Galactic latitude b is -7.7 degrees. Based on the IRAS colours and flux distribution it is classified as a post-AGB star. This star does not have accurate *Gaia* DR2 parallax.

- IRAS 18075-0924

It is a high velocity star. *Gaia* DR2 parallax is not accurate. Spectroscopic and photometric study of this star is needed. Based on IRAS colours and flux distribution it is classified as a post-AGB candidate.

4 Discussion and concluding remarks

4.1 Populations of post-AGB stars with high radial velocities

Nine objects in our sample, HD 46703, HD 56126, IRAS 07140–2321, IRAS 08187–1905, HD 116745, IRAS 14325–6428, HD 137569, BD+33°2642, and IRAS 17436+5003 are identified as post-AGB stars with high radial velocities (tables 1 and 2). The very luminous object BD-12

4970 is discussed separately. Their computed absolute luminosities and comparisons with post-AGB evolutionary track (Figure 2) indicates that their initial main-sequence mass is less than 2 solar masses. Among them, only two stars, HD 116745 and BD+33°2642, clearly belong to the galactic halo population (table 3, figure 1). IRAS 07140-2321 has the largest L_z and E (table 3). The other six post-AGB stars are not separated from disk stars in figures 1 and 2, although they have relatively high radial velocity. This indicates that the criterion of the radial velocity ($|V_{\text{Helio}}| > 45 \text{ km s}^{-1}$) is not sufficient to effectively select halo post-AGB stars. The radial velocities of the clear examples of halo objects identified by this work, HD 116745 and BD+33°2642, are $V_{\text{Helio}} = 240$ and -94 km s^{-1} , respectively. It should be noted that the above criterion is adopted in this work as we do not miss halo objects from the sample of Vickers et al. (2015).

IRAS 07140-2321 is a unique object that has high total energy of the orbital motion and high z -component of angular momentum. The star seems to belong to the disk population rather than the halo from the prograde rotation with small v_R and v_z . The distance and the high total energy suggests that it is a outer disk object.

BD−12°4970 (LS IV -12 13) is a hot high velocity star with accurate parallax. Its computed absolute luminosity indicates that its initial main-sequence mass may be 4.0 solar masses. The kinematics of this object suggest this object belongs to disk population.

Among the objects studied in Parthasarathy et al. (2020), three objects (LS 3593, LSE 148, and HD 214539) have clear kinematics features of halo objects (figure 1), whereas those of three other stars are not distinguished from disk stars. Another object, LS 5107, has high total energy of the orbital motion and high z -component of angular momentum, as found for IRAS 07140-2321 in the current sample. As LSE 148 is less luminous objects, the clear halo post-AGB stars identified by the study is LS 3593 and HD 214539.

4.2 Comments for other objects

The two less luminous stars HD 178443 and PHL 1580 also belong to the halo population (figure 1). The high velocity hot metal-poor star PHL 1580 with accurate parallax is found to have very low luminosity (table 2) compared to post-AGB stars. It may be a hot sub-dwarf star. LSE 182 (HD 178443) is a high velocity metal-poor star in the Galactic halo and could be a red HB star (McWilliam et al. 1995).

BD+32°2754 also has low absolute luminosity. It may be a sub-dwarf. IRAS 07227−1320 with the spectral type M1 may be a cool post-AGB star. It needs further study to understand its

chemical composition and evolutionary stage. The computed absolute luminosity of post-AGB star HD 161796 (tables 2) and its location in figure 2 indicates that its initial main-sequence mass may be in the range around 2 solar masses.

Kamath et al. (2015) found dusty post-red giant branch (post-RGB) stars in LMC and SMC. They found that these stars have mid-IR excesses and stellar parameters (T_{eff} , $\log g$, [Fe/H]) similar to those of post-AGB stars, but their luminosities are less than $2500 L_{\odot}$. Their lower luminosities indicate they have lower masses and radii. Some of the stars in our sample also have luminosities less than $2500 L_{\odot}$ (table 2, figure 2) and they may be post-RGB stars similar to those found by Kamath et al. (2015). The very low luminosity stars like PHL 1580 mentioned above is a puzzle. They may be post-HB stars or evolving towards AGB-manque star stage.

Recently, Bond (2020) found BD+14°3061 to be a luminous, metal-poor, yellow post-AGB supergiant star in the galactic halo. He found it to be a a very high-velocity star moving in a retrograde Galactic orbit. It is not an IRAS source. The Galactic halo post-AGB stars have relatively low core-mass. They evolve slowly and, by the time they evolve to G and F-type post-AGB stage, their circumstellar dust shells get dispersed into the interstellar medium. They never become PNe. The galactic halo post-AGB supergiants are very rare. Discovering them is a challenging task. Bond (2020) derived absolute visual magnitude M_V of this star from *Gaia* DR2 parallax to be $M_V = -3.44$. Since its bolometric correction is close to zero (i.e., $M_V = M_{\text{bol}}$), Bond (2020) proposed that these Galactic halo A and F-supergiants are useful as standard candles as they are luminous and have same absolute luminosity. Some of the galactic halo post-AGB stars in our sample seems to be similar to BD+14°3061. Extensive survey is needed to detect more galactic halo post-AGB supergiants.

5 Summary

This paper investigates the list of post-AGB star candidates of Vickers et al. (2015) selecting objects with high radial velocities. We identify two clear examples of high-velocity low-mass post-AGB stars and a few candidates from the evolutionary status and kinematics information derived from the *Gaia* DR2 and EDR3. Through the studies of this paper and of the previous one (Parthasarathy et al. 2020), four clear halo post-AGB stars are identified (HD 116745, BD+33°2642, LS 3525 and HD 214539). We also find that the list of Vickers et al. (2015) include objects which are not classified into post-AGB stars, taking the new estimate of luminosity based on parallax measurements with *Gaia*. Further studies of the sample of Vickers et al.

(2015) with spectroscopy to determine radial velocities are useful to obtain statistics of post-AGB stars as well as information on individual objects.

Acknowledgments

MP was supported by the NAOJ Visiting Fellow Program of the Research Coordination Committee, National Astronomical Observatory of Japan (NAOJ), National Institutes of Natural Sciences(NINS).

References

- Bailer-Jones, C. A. L., Rybizki, J., Fouesneau, M., et al. 2021, *AJ*, 161, 147. doi:10.3847/1538-3881/abd806
- Bennett, M. & Bovy, J. 2019, *MNRAS*, 482, 1417. doi:10.1093/mnras/sty2813
- Bond, H. E. 2020, *AJ*, 160, 274. doi:10.3847/1538-3881/abc177
- Brunthaler, A. 2004, Ph.D. Thesis, Max-Planck-Institut für Radioastronomie
- Casagrande, L., & VandenBerg, D. A. 2018, *MNRAS*, 479, L102
- Casagrande, L., Wolf, C., Mackey, A. D., et al. 2019, *MNRAS*, 482, 2770. doi:10.1093/mnras/sty2878
- Chen, B.-Q., Huang, Y., Yuan, H.-B., et al. 2019, *MNRAS*, 483, 4277
- Cox, A. N. 2000, *Allen's Astrophysical Quantities*
- De Smedt, K., Van Winckel, H., Kamath, D., et al. 2016, *A&A*, 587, A6. doi:10.1051/0004-6361/201527430
- De Smedt, K., Van Winckel, H., Karakas, A. I., et al. 2012, *A&A*, 541, A67. doi:10.1051/0004-6361/201219150
- Dorman, B., Rood, R. T., & O'Connell, R. W. 1993, *ApJ*, 419, 596
- Flower, P. J. 1996, *ApJ*, 469, 355
- Fujii, T., Nakada, Y., & Parthasarathy, M. 2002, *A&A*, 385, 884. doi:10.1051/0004-6361:20020178
- Gaia Collaboration, Brown, A. G. A., Vallenari, A., et al. 2018, *A&A*, 616, A1
- Gielen, C., Bouwman, J., van Winckel, H., et al. 2011, *A&A*, 533, A99. doi:10.1051/0004-6361/201117364
- Gonzalez, G. & Wallerstein, G. 1992, *MNRAS*, 254, 343. doi:10.1093/mnras/254.2.343
- Green, G. M., Schlafly, E. F., Finkbeiner, D., et al. 2018, *MNRAS*, 478, 651
- Hardorp, J., Theile, I., & Voigt, H. H. 1964, *Hamburger Sternw. Warner & Swasey Obs.*, C03
- Hrivnak, B. J., Van Winckel, H., Reyniers, M., et al. 2008, *AJ*, 136, 1557. doi:10.1088/0004-6256/136/4/1557
- Iben, I. & Renzini, A. 1983, *ARA&A*, 21, 271. doi:10.1146/annurev.aa.21.090183.001415

Iyengar, K. V. K. & Parthasarathy, M. 1997, *A&AS*, 121, 45. doi:10.1051/aas:1997111

Jurić, M., Ivezić, Ž., Brooks, A., et al. 2008, *ApJ*, 673, 864

Kamath, D., Wood, P. R., & Van Winckel, H. 2015, *MNRAS*, 454, 1468. doi:10.1093/mnras/stv1202

Kamath, D. & Van Winckel, H. 2022, *Universe*, 8, 233. doi:10.3390/universe8040233

Kamath, D., Van Winckel, H., Ventura, P., et al. 2022, *ApJL*, 927, L13. doi:10.3847/2041-8213/ac5686

Kwok, S., Volk, K. M., & Hrivnak, B. J. 1989, *ApJL*, 345, L51. doi:10.1086/185550

Lindgren, L., Hernández, J., Bombrun, A., et al. 2018, *A&A*, 616, A2

Lindgren, L., Klioner, S. A., Hernández, J., et al. 2021, *A&A*, 649, A2. doi:10.1051/0004-6361/202039709

Luck, R. E. & Bond, H. E. 1984, *ApJ*, 279, 729. doi:10.1086/161939

Luck, R. E., Bond, H. E., & Lambert, D. L. 1990, *ApJ*, 357, 188. doi:10.1086/168904

Martin, J. C. 2004, *AJ*, 128, 2474. doi:10.1086/425045

Martin, J. C. 2006, *AJ*, 131, 3047. doi:10.1086/504079

McCausland, R. J. H., Conlon, E. S., Dufton, P. L., et al. 1992, *ApJ*, 394, 298. doi:10.1086/171582

McMillan, P. J. 2017, *MNRAS*, 465, 76

McWilliam, A., Preston, G. W., Sneden, C., et al. 1995, *AJ*, 109, 2757. doi:10.1086/117486

Miller Bertolami, M. M. 2016, *A&A*, 588, A25

Napiwotzki, R., Heber, U., & Koepfen, J. 1994, *A&A*, 292, 239

Omont, A., Loup, C., Forveille, T., et al. 1993, *A&A*, 267, 515

Oomen, G.-M., Van Winckel, H., Pols, O., et al. 2018, *A&A*, 620, A85. doi:10.1051/0004-6361/201833816

Parthasarathy, M. 1993, *ApJL*, 414, L109. doi:10.1086/187008

Parthasarathy, M. 1993, *Luminous High-Latitude Stars*, 45, 173

Parthasarathy, M. 2022, *Research Notes of the American Astronomical Society*, 6, 33. doi:10.3847/2515-5172/ac54bb

Parthasarathy, M. & Pottasch, S. R. 1989, *A&A*, 225, 521

Parthasarathy, M. & Pottasch, S. R. 1986, *A&A*, 154, L16

Parthasarathy, M., Matsuno, T., & Aoki, W. 2020, *PASJ*, 72, 99. doi:10.1093/pasj/psaa097

Parthasarathy, M., Garcia Lario, P., & Pottasch, S. R. 1992, *A&A*, 264, 159

Pottasch, S. R. & Parthasarathy, M. 1988, *A&A*, 192, 182

Preite-Martinez, A. 1988, *A&AS*, 76, 317

Rao, S. S., Giridhar, S., & Lambert, D. L. 2012, *MNRAS*, 419, 1254. doi:10.1111/j.1365-2966.2011.19780.x

Reddy, B. E. & Parthasarathy, M. 1996, *AJ*, 112, 2053. doi:10.1086/118162

- Reid, M. J., & Brunthaler, A. 2004, *ApJ*, 616, 872
- Schoenberner, D. 1983, *ApJ*, 272, 708. doi:10.1086/161333
- Schlafly, E. F., & Finkbeiner, D. P. 2011, *ApJ*, 737, 103
- Schlegel, D. J., Finkbeiner, D. P., & Davis, M. 1998, *ApJ*, 500, 525
- Schönrich, R., Binney, J., & Dehnen, W. 2010, *MNRAS*, 403, 1829. doi:10.1111/j.1365-2966.2010.16253.x
- Sharma, S., Hayden, M. R., Bland-Hawthorn, J., et al. 2021, *MNRAS*. doi:10.1093/mnras/stab1086
- Stassun, K. G. & Torres, G. 2021, *ApJL*, 907, L33. doi:10.3847/2041-8213/abdaad
- van Winckel, H. 2003, *ARA&A*, 41, 391. doi:10.1146/annurev.astro.41.071601.170018
- Van Winckel, H., Jorissen, A., Exter, K., et al. 2014, *A&A*, 563, L10. doi:10.1051/0004-6361/201423650
- Vickers, S. B., Frew, D. J., Parker, Q. A., et al. 2015, *MNRAS*, 447, 1673. doi:10.1093/mnras/stu2383

Table 1. Basic data of twenty high velocity post-AGB candidates

star	l (deg)	b (deg)	Sp.	V	G	$(B - V)$	$(B - V)_0$	$E(B - V)$				T_{eff} (K)	B.C	Ref.
								Sp	Sp	SFD	3D			
1)IRAS 02143+5852	133.8	-1.93	F7Ie	13.8	13.51	1.22	0.48	0.74	1.05		...	6000	-0.07	1,2,3
2)IRAS 05089+0459	196.3	-19.5	M3I	14.08	13.13	1.74			0.14		...	3200	-2.24	1,4
3)IRAS 05208-2035	222.8	-28.3		9.48	8.98	1.04	0.7:	0.3:	0.06	0.08	0.3±0.2	4900	-0.33	5,6,7
4)HD 46703 (IRAS 06338+5333)	162.0	+19.	F7I	9.04	8.84	0.48	0.02	0.46	0.08	0.10	0.46±0.20	6000	-0.06	1,7,8,9
5)HD 56126 (IRAS 07134+1005)	206.7	+10.0	F5Ia	8.32	8.06	0.88	0.32	0.56	0.08	0.00	0.56±0.20	6500	-0.03	1,10,11,12
6)IRAS 07140-2321	236.6	-5.4	F5I	10.73	10.49	0.43	0.23	0.20	0.59	0.57	0.57±0.20	7000	0.0	1,13
7)IRAS 07227-1320	228.7	+1.2	MII	12.55	11.6	1.96	1.69	0.27	0.51	0.43	0.43±0.20	3500	-1.45	1,14
8)IRAS 08187-1905	240.6	+9.8	F6Ib/II	9.02	8.83	0.61	0.40	0.21	0.11	0.15	0.21±0.05	6150	-0.06	1,12,15
9)HD 116745	309.1	+15.2	A7/A9e	10.79	10.68	0.29	0.13	0.16	0.13		0.16±0.05	6950	-0.0	1,16
10)IRAS 14325-6428	313.9	+4.1	F5I	12.0	11.27	0.56	0.32	0.24	0.64	0.89	0.89±0.20	6400	-0.03	1,11,12
11)IRAS 15210-6554	317.7	-7.7	K2I	11.85	11.72	(0.03)*	1.36		0.20		...	4310	-0.61	1
12)HD 137569	21.9	+51.9	B9Iab:p	7.91	7.89	-0.05	...	0.0	0.05	0.01	0.01±0.05	10,500	-0.53	1,17,18
13)BD+33 2642	52.7	+50.8	O7p	10.73	10.78	-0.12	-0.27	0.15	0.02	0.06	0.15±0.05	20,000	-1.66	1,19,20
14)BD+32 2754	53.6	+41.5	F8	9.55	9.46	0.57	0.56	0.01	0.02	0.02	0.01±0.05	5750	-0.09	1,14
15)HD161796 (IRAS 17436+5003)	77.1	+30.9	F3Ib	7.21	7.08	0.47	0.26	0.21	0.03	0.04	0.21±0.05	6500	-0.03	1,9,12,21
16)BD-12 4970	018.0	+1.6	B0.5Ia	8.78	8.30	1.02	-0.21	1.23	2.71	1.58	1.23±0.20	27,000	-2.40	1
17)IRAS 18075-0924	019.8	+4.7	—	13.9	12.47	1.4			1.41		...			1
18)HD 178443	354.2	-21.5	F8	10.02	9.80	0.673	0.56	0.11	0.09		0.11±0.05	5180	-0.09	1,22
19)PHL 1580	031.3	-43.5	B0I	12.33	12.19	(0.14)*	-0.22		0.04	0.03	0.03±0.05	24,000	-2.8	1,23
20)LS III +52 5	095.1	+0.8	OB-	(12.2)*	11.74	(0.46)*	-0.22		2.91	0.03	0.03±0.05	25,000	-2.9	1,24

Notes:- (*) indicates (V-R) for 11)IRAS 15210-6554, (V-G) for 19)PHL 1580, and B mag and (B-G) for 20)LS III +52 5. $E(B - V)_{\text{Sp}}$ indicates $(B - V) - (B - V)_0$, where $(B - V)_0$ is estimated from the spectral type. $E(B - V)_{\text{SFD}}$ is from the 2D dust extinction map of Schlegel et al. (1998). $E(B - V)_{\text{3D}}$ is taken from 3D dust maps of Green et al. (2019) if $|b| > 10^\circ$ and Chen et al. (2019) if $|b| < 10^\circ$.
References: 1)SIMBAD; 2)Fujii et al. (2002); 3)Omont et al. (1993); 4)Iyengar & Parthasarathy (1997); 5)Gielen et al. (2011); 6)Rao et al. (2012); 7)Oomen et al. (2018); 8)Luck & Bond (1984); 9)Parthasarathy & Pottasch (1986); 10)Parthasarathy et al. (1992); 11)De Smedt et al. (2016); 12)Kamath et al. (2022); 13)Gielen et al. (2011); 14)Vickers et al. (2015); 15)Reddy & Parthasarathy (1996); 16)Gonzalez & Wallerstein (1992); 17)Martin (2004); 18)Martin (2006); 19)Napiwotzki et al. (1994); 20)Van Winckel et al. (2014); 21)Luck et al. (1990); 22)McWilliam et al. (1995); 23)McCausland et al. (1992); 24)Hardorp et al. (1964)

Table 2. Gaia DR2 parallaxes and derived luminosities of twenty high velocity post-AGB candidates

Star	parallax*	Distance	Distance (BJ)	$\log(L/L_{\odot})^{\ddagger}$	$\log(T_{\text{eff}}/\text{K})$	RV [†]	RUWE	Subsection
	(mas)	(kpc)	(kpc)			(km s ⁻¹)		in Sect. 3
1)IRAS 02143+5852	1.364±0.289	>0.510		>0.74	3.778	-49.02±14.69	18.689	3.4
2)IRAS 05089+0459	0.754±0.345	>0.684		>0.88	3.477	85.92±1.49	21.908	3.4
3)IRAS 05208-2035	0.687±0.030	1.420±0.064	1.403 ^{+0.053} _{-0.059}	2.91±0.25	3.690	52.84±3.68	2.184	3.4
4)HD 46703	0.268±0.024	3.512±0.330	3.399 ^{+0.276} _{-0.278}	3.92±0.26	3.778	-83.53±7.71	1.622	3.2
5)HD 56126	0.454±0.024	2.124±0.114	2.099 ^{+0.108} _{-0.110}	3.93±0.25	3.813	93.71±3.54	0.922	3.1
6)IRAS 07140-2321	0.178±0.012	5.116±0.343	5.122 ^{+0.377} _{-0.404}	3.74±0.26	3.845	62.38±4.13	1.029	3.1
7)IRAS 07227-1320	0.489±0.021	1.975±0.087	1.982 ^{+0.068} _{-0.073}	2.58±0.25	3.544	70.68±0.39	1.176	3.3
8)IRAS 08187-1905	0.288±0.033	3.280±0.403	3.259 ^{+0.342} _{-0.391}	3.60±0.12	3.789	65.44±1.87	1.695	3.2
9)HD 116745	0.177±0.020	5.154±0.597	4.893 ^{+0.379} _{-0.444}	3.20±0.11	3.842	240.11±0.54	0.933	3.1
10)IRAS 14325-6428	0.192±0.037	4.795±1.033	4.883 ^{+0.622} _{-0.928}	2.77±0.30	3.806	-76.54±10.08	2.181	3.2
11)IRAS 15210-6554	-0.152±0.143	>6.623		>3.29	3.634	-83.90±0.87	2.279	3.4
12)HD 137569	0.752±0.079	1.301±0.150	1.316 ^{+0.132} _{-0.197}	3.19±0.11	4.021	-45.0	2.023	3.2
13)BD+33 2642	0.271±0.032	3.474±0.434	3.467 ^{+0.308} _{-0.466}	3.54±0.12	4.301	-94.7±2.5	1.295	3.1
14)BD+32 2754	3.239±0.014	0.307±0.001	0.307 ^{+0.001} _{-0.001}	1.10±0.06	3.760	-60.50±0.50	1.161	3.3
15)HD 161796	0.502±0.024	1.926±0.091	1.921 ^{+0.091} _{-0.095}	3.85±0.07	3.813	-54.17±1.78	1.216	3.1
16)IRAS 18075-0924	-0.171±0.192	>4.348				-59.68±0.68	7.580	3.4
17)BD-12 4970	0.467±0.020	2.065±0.090	1.984 ^{+0.072} _{-0.101}	5.50±0.25	4.431	124.95±9.43	0.956	3.1
18)HD 178443	1.034±0.016	0.951±0.014	0.939 ^{+0.014} _{-0.015}	1.99±0.06	3.714	343.55±0.28	1.102	3.3
19)PHL 1580	3.156±0.018	0.315±0.002	0.314 ^{+0.001} _{-0.002}	1.12±0.06	4.380	-70.53±0.72	0.954	3.3
20)LS III +52 5	3.119±0.011	0.319±0.001	0.315 ^{+0.001} _{-0.001}	1.22±0.06	4.398	-232.83±0.67	0.817	3.3

* From Gaia EDR3 (Lindegren et al. A&A, 2021, in press. arxiv:2012.03380).

† From Gaia DR2 except for IRAS 07140-2321, HD 137569, and BD+33 2642, for which the values are respectively taken from RAVE DR6 (Steinmetz et al. 2020, AJ, 160, 82), Dulflot et al. (1995, A&AS,114, 269), and Gontcharov, G. A.(2006, Astronomy Letters, 32, 759).

‡ The luminosity uncertainty includes the uncertainty in distance and reddening (§ 2). In case the relative parallax measurement uncertainty is larger than 20%, we provide 2 σ lower limits.

Table 3. Kinematics information of twenty high velocity post-AGB candidates

	v_T^*	v_ϕ	v_R	v_z	L_z	E
	(km s ⁻¹)	(km s ⁻¹)	(km s ⁻¹)	(km s ⁻¹)	(kpc km s ⁻¹)	(km ² s ⁻²)
1)IRAS 02143+5852	>8.6					
2)IRAS 05089+0459	>18.5					
3)IRAS 05208-2035	16.2	216.3	13.0	-4.9	1983.8	-153156
4)HD 46703	66.5	162.6	-51.8	-17.7	1857.2	-149824
5)HD 56126	5.1	207.8	52.1	18.9	2104.9	-148503
6)IRAS 07140-2321	63.0	240.1	-11.9	-3.8	2839.3	-134521
7)IRAS 07227-1320	15.0	206.9	15.1	8.0	1992.9	-152988
8)IRAS 08187-1905	36.9	207.3	-8.7	-1.0	2119.8	-149469
9)HD 116745	185.4	-84.6	-56.6	-74.8	-541.3	-184843
10)IRAS 14325-6428	207.3	241.2	55.9	44.0	1457.7	-167529
11)IRAS 15210-6554	>273.0					
12)HD 137569	90.9	226.4	-50.2	-79.3	1688.5	-156543
13)BD+33 2642	238.3	13.5	142.2	85.1	98.0	-169581
14)BD+32 2754	66.9	159.4	20.9	12.8	1286.9	-170975
15)HD 161796	109.6	193.8	-69.7	-17.5	1551.1	-161792
16)BD-12 4970	27.0	272.0	-111.3	3.6	1706.0	-154487
17)IRAS 18075-0924	>137.4					
18)HD 178443	233.1	-21.9	-300.4	-131.0	-160.5	-135111
19)PHL 1580	47.6	186.6	51.6	24.1	1495.6	-165370
20)LS III +52 5	79.7	7.0	33.3	-42.0	57.6	-181508

* Tangential velocity computed from the proper motion and parallax. In case the relative parallax measurement uncertainty is larger than 20%, we provide 2σ lower limit.

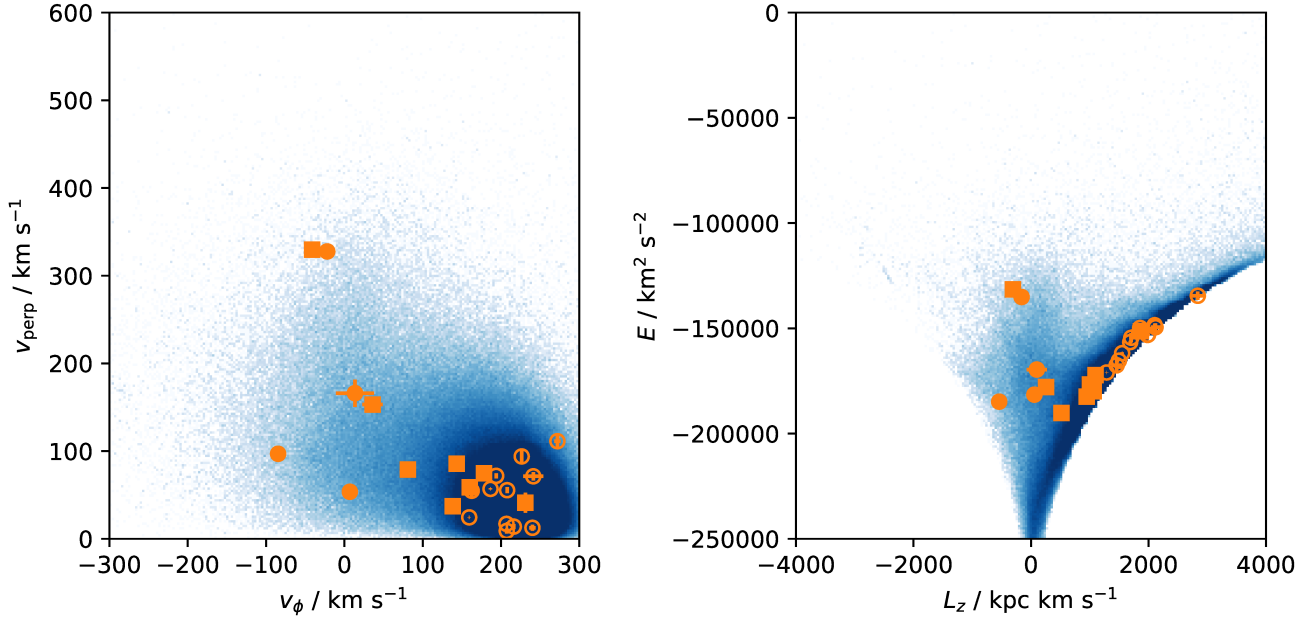


Fig. 1. Kinematics of the post-AGB candidates in the present study in the Galactocentric frame. The four objects with halo kinematics found by the present work are shown by filled circles, whereas those with disk-like kinematics are shown by open circles. The filled squares are the objects included in Parthasarathy et al. (2020).

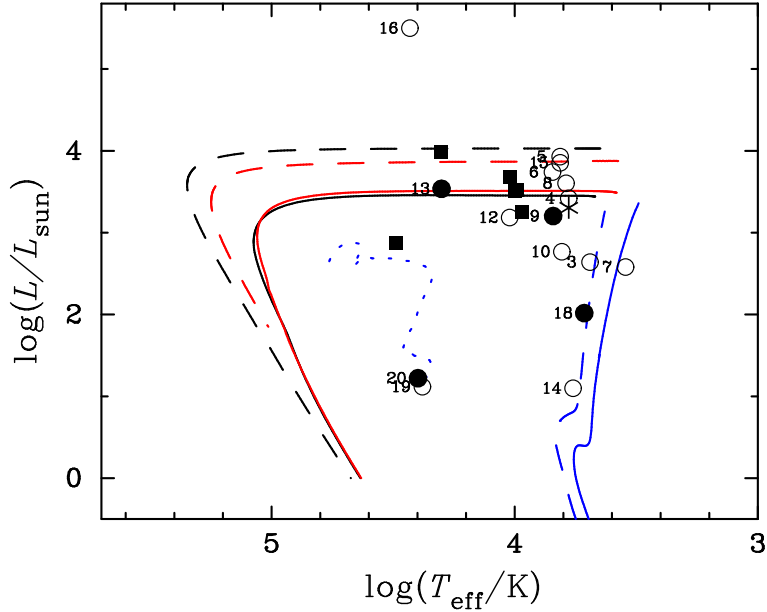


Fig. 2. Evolutionary tracks of post-AGB phases taken from Miller Bertolami (2016) for initial masses of $1.0 M_{\odot}$ (solid lines) and $2.0 M_{\odot}$ (dotted lines) with $Z = 0.02$ (red) and $Z = 0.001$ (black). The evolutionary track of post-HB star for the core mass of $0.52 M_{\odot}$ with $[\text{Fe}/\text{H}] = -1.48$ taken from Dorman et al. (1993) is shown by dotted (blue) line. The isochrones of Yonsei-Yale models for the age of 9 Gyr are shown by (blue) solid and dashed lines for $[\text{Fe}/\text{H}] = 0.0$ and -1.7 , respectively, presenting the red giant branches. The four objects with halo kinematics found by the present work are shown by filled circles, among which HD 116745 and BD+33° 2642 are clearly post-AGB stars. Other 12 objects with reliable luminosity are shown by open circles. The object numbers given in the tables are presented. The five objects reported in Figure 1 of Parthasarathy et al. (2020) are plotted by filled squares. The post-AGB star BD+14° 3061 is plotted by asterisk, adopting $T_{\text{eff}} = 6000 \text{ K}$ (Bond 2020).